Novel three-piston pump design for a slipper test rig

Junhui Zhang[a], Qun Chao[a], Bing Xu[a,*], Min Pan[b], Qiannan Wang[a], Yuan Chen[a]

[a]State Key Laboratory of Fluid Power and Mechatronic Systems, Zhejiang University, Hangzhou, China

[b]Department of Mechanical Engineering, University of Bath, Bath, United Kingdom

*Corresponding Author: bxu@zju.edu.cn

Abstract

Slipper's micro motions including the squeezing motion, spinning motion, and tilting motion have a significant impact on its lubricating condition and dynamic behavior. However, few experimental studies are on these micro motions within a real axial piston pump, especially the slipper's spinning motion. The experimental investigations on the slipper in the past mainly focused on the parameters of the oil film such as pressure, thickness, and temperature. The sensors were often installed in the fixed swash plate when the cylinder block was chosen to rotate. Alternatively, the sensors were mounted in the fixed modified slipper when the swash plate rotated. The biggest challenge of the direct measurements of these micro motions is the space limitation for the sensor installation due to the compact structure of axial piston pumps as well as the slipper's macro motion. This paper presents a new three-piston pump for the slipper test rig which can provide enough installation space for the sensor. To realize the cylinder block balance, a hold-down plate is first introduced into this three-piston pump. In addition, a detailed set of relevant equations is derived to evaluate the functionality of the hold-down plate. Finally, the slipper's spinning motion was measured directly and continuously using this three-piston pump, which confirmed the capability of the slipper test rig.

Keywords: Three-piston pump; Slipper test rig; Spinning motion measurement

1. Introduction

Axial piston pumps are widely used to provide hydraulic power for the hydraulic circuit because of their high pressure, high efficiency, high power density and convenient flow regulation [1]. When the pump operates, thin oil film forms within the three main lubricating interfaces, the slipper/swash plate interface, the piston/cylinder block interface, and the cylinder block/valve plate interface, as shown in Fig. 1. These interfaces act as both bearing function and sealing function, which determine the pump reliability, robustness, and efficiency. Specifically, they have to bear the external forces acting on the components of friction pairs. On the other hand, these lubricating interfaces need to seal the gaps to prevent the pressurized fluid from flowing into the pump case, i.e., the leakage flows from the displacement chamber through the slipper/swash plate interface (Q_{SS}), the piston/cylinder block interface (Q_{PB}), and the cylinder block/valve plate interface (Q_{BV}) to the pump case.

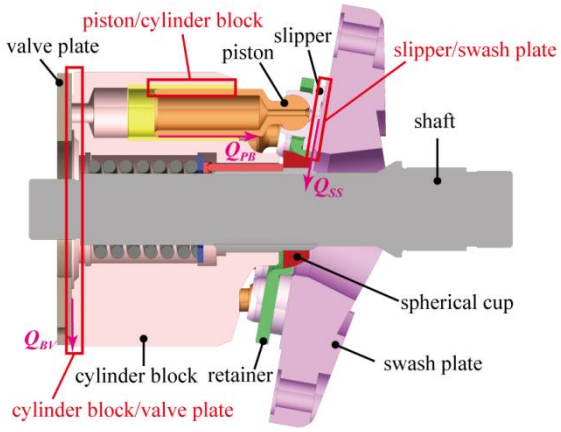

Fig. 1. Main lubricating interfaces within an axial piston pump

In the last forty years, a considerable amount of theoretical and experimental work has been carried out on the

slipper/swash plate lubricating interface. Iboshi and Yamaguchi [2,3] investigated theoretically and experimentally the lubrication characteristics of the slipper/swash plate interface considering all the oil-film parameters including the tilting angle, maximum tilting angle azimuth, and mean oil-film thickness. Yabe and Kubo [4] clarified the generation mechanism of load-carrying capacity for the over-clamped slipper. They evaluated the slipper attitude that was characterized by the oil-film thickness and tilting angle under the quasi static condition. Tanaka et al. [5] examined the motion characteristics of the slipper bearing for which a mathematical model considering the asperity contacts of surface roughness was developed. Their proposed model was validated through measuring the oil-film thickness between the swash plate and slipper. Borghi et al. [6] presented a numerical model for the dynamic behavior prediction of an over-clamped slipper, in which the slipper spin was taken into account. Using this numerical model, the effects of the slipper spin on the central oil-film thickness, tilting angle, and azimuth of the minimum oil-film thickness were analyzed. Lin and Hu [7] presented a tribo-dynamic model of the slipper bearing which coupled the slipper's tribological and dynamical behaviors. The influence of the operating conditions on the oil-film thickness was evaluated. A slipper test rig was built to measure the oil-film thickness of the slipper bearing, and the measured results agreed well with the theoretical analysis. Harris et al. [8] established a dynamic model to predict the slipper's motion with respect to the swash plate. It was revealed that the slipper's tilting behavior increased with the pump speed, resulting in a potential metal-to-metal contact between the slipper and swash plate or retainer. Similarly, Manring [9] presented the governing equations for predicting the slipper's tilting motion. He pointed out that the slipper's tilting motion was most likely to take place at the transition region from the discharge side to the suction side. Borghi et al. [10] derived the critical pump speed at which the slipper started to tilt away from the swash plate. Hooke et al. [11-13] studied the lubrication characteristics of the slipper bearing with different running surface profiles theoretically and experimentally. It was discovered that a certain amount of non-flatness of the slipper's running surface was essential for successful slipper operation. Xu et al. [14] carried out numerical and experimental studies on the slipper's partial abrasion phenomenon, and found that an optimal slope on the inner edge of the sealing land was helpful to improve the load-carrying capacity of slipper and reduce the partial abrasion.

To achieve higher power density, the continued development of axial piston pumps has put an increasing demand for greater speeds and pressures. However, the strengthened fluid-structure-thermal coupling effect will be encountered when axial piston pumps operate under high-pressure and high-speed conditions, which causes local pressure deformation and thermal deformation of movable parts [15]. The Maha Fluid Power Research Center in Purdue University conducted some of the most pioneering work in which a fully coupled fluid-structure-thermal model for the slipper bearing in swash-plate type axial piston pumps was developed based on the sophisticated simulation tool CASPAR [16-18]. Similarly, Tang et al. [19] developed a thermos elasto hydro dynamic (TEHD) lubrication model for the slipper bearing in axial piston pumps, which considered the coupling between the elasto hydro dynamic behavior and viscosity temperature effect.

The slipper test rig is an essential aspect of experimental research on the lubrication characteristics of the slipper bearing. Actually, there are also many test rigs for the piston/cylinder block interface and cylinder block/valve plate interface. Among these three lubricating interfaces, the cylinder block/valve plate interface seems to be the most easily investigated experimentally since it has relatively large space for the sensor installation. Kim et al. [20] used a test pump to measure the oil-film thickness between the cylinder block and valve plate. The displacement sensor was installed in a hole located at the cylinder block to continuously measure the oil-film thickness. The wire of the sensor was carefully led through the hollow shaft and taken out through the center of the fixed valve plate and rear housing. During cylinder block rotation, the signals received from the sensor were transmitted to a recorder by means of a slip ring unit. In reality, the valve plate is fixed on the pump housing where it can provide enough space for the sensor installation. This makes it possible to obtain the measured data from the stationary sensor without signal transmission from a moving part to a stationary part. The second method is more convenient and reliable but at the expense of non-continuous measurements of the oil-film thickness. Bergada et al. [21] adopted the second measurement method and installed three position transducers in the valve plate to capture the oil-film thickness of three different positions within the cylinder block/valve plate interface. Similarly, Wegner et al. [22] employed several eddy current sensors located at fixed positions with respect to the valve plate to measure micro motions of the cylinder block within a modified axial piston pump.

The piston/cylinder block interface has a different relative motion of its two members since both the piston and

cylinder block are in motion while the valve plate and swash plate remain stationary. Tanaka et al. [23] built a test device for measuring the friction force acting on the piston and the piston's spinning speed within the cylinder block. However, the centrifugal force of the piston-slipper assembly was neglected because the test device used an inverse kinematics, in other words the swash plate rotated relative to the stationary cylinder block. Similar methods of inverse kinematics for building the piston test rig were also adopted by Manring [24], and Scharf and Murrenhoff [25], which all failed to take into account the centrifugal force of the piston-slipper assembly. In order to realize oil-film measurements within the piston/cylinder block interface based on realistic kinematics, Olems [26] created a model pump to measure the temperature distribution in the piston/cylinder block interface by modifying a commercial axial piston pump. This model pump provided a possibility to produce instantaneous displacement chamber pressure, and successfully achieved the goal of cylinder block rotation relative to the swash plate. The problem associated with the data transmission from the rotating cylinder block was solved by means of telemetry. The same measurement strategy was also adopted by Ivantysynova and Lasaar [27], who developed another model pump called "tribo pump" to measure the piston friction forces under real operating conditions.

Swash plate has a relatively large surface area for installing sensors. Moreover, it can have a fixed inclined angle with respect to the cylinder block when the slippers slide on the swash plate. This makes it possible to obtain the data from the sensors without signal transmission using telemetry or slip ring unit. Tang et al. [28] employed eight displacement sensors and four thermocouples to measure the oil-film thickness and temperature within the slipper/swash plate interface. These displacement sensors and thermocouples were installed in the modified swash plate along the motion trajectory of the slipper to capture the oil-film thickness and temperature. Spencer [29] utilized the similar measurement concept in a test pump where six sensors were embedded in the modified swash plate. He accomplished the measurements of the oil-film thickness between the slipper and swash plate using this test pump. It is worth mentioning that this modified pump could behave like a real pump and operate at speed of 2000 rpm and system pressure up to 35 MPa. Although these two slipper test rigs could realize minimal alterations to the original pump components to maintain the oil-film measurement integrity, they had the disadvantage of non-continuous measurement because each sensor was active only when the test slipper reached the specified position on the swash plate.

There are two main reasons for using the intermittent measurement method when designing slipper test rigs. The first reason is that the continuous measurements often involve the problem of transmitting sensor signals from a moving part. This problem can be solved by using a slip ring unit [20] or telemetry technology [26,27], but this method makes the experiments more costly and less reliable. The second reason is that there is not enough space to mount sensors on the movable parts such as slipper and retainer due to the compact structure of commercial axial piston machines, as shown in Fig. 2. There is a dilemma in attempting to redesign the axial piston pump for the sensor installation. The slipper test rig requires the redesigned axial piston pump to provide enough space for the sensor installation. Reducing the number of pistons is an effective way to obtain a larger installation space. However, on the other hand, it is desirable that the redesigned axial piston pump can have sufficient pistons and behave like a real one so that it can maintain the measurement integrity.

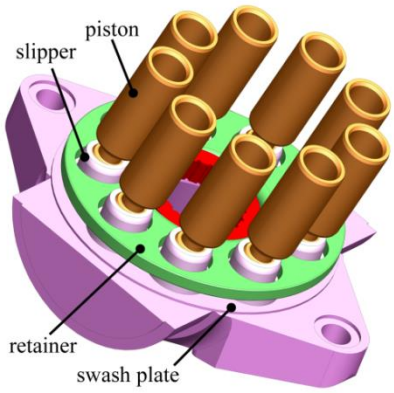

Fig. 2. Slipper/swash plate interface within an axial piston pump

Additionally, the consideration of cylinder block balance is another reason behind the demand on pistons within the

test pump. There are two main axial forces acting on the cylinder block. One of these forces is the hydrostatic separating force due to the pressure in the discharge and intake ports and across their sealing lands, which tends to separate the cylinder block from the valve plate. The other axial force is the displacement chamber pressure force, which attempts to push the cylinder block towards the valve plate. The hydrostatic separating force is likely to be much larger than the displacement chamber pressure force when the number of pistons within an axial piston pump is reduced. It is therefore not possible to achieve cylinder block balance if the remaining separating force cannot be counteracted. In addition, the cylinder block is subject to a fluid moment due to the pressure distribution along the discharge side and intake side. If the number of pistons is not sufficient, the fluid moment cannot be entirely balanced by the displacement chamber pressure. As a result, the cylinder block tilts away from the valve plate, leading to an increase in leakage losses and potential metal-to-metal contact across the cylinder block/valve plate interface.

This paper aims to design a novel three-piston pump for the slipper test rig. The reduced number of pistons provides a possibility to offer enough space for sensor installation. Especially, a hold-down device for the cylinder block is first created and introduced to the modified axial piston pump, which helps to balance the remaining separating force and tilting moment acting on the cylinder block. Finally, the measurement of slipper spinning motion will be present as an example to verify the proposed three-piston pump design.

2. Machine Description

Fig. 3 shows the main configuration of the three-piston pump, where totally six piston bores are spaced evenly about the shaft centerline in a circular array within the cylinder block, but only three active piston bores are in service for the purpose of providing more space for sensor installation. The other three inactive piston bores mainly offer additional potential for weight saving, and they are not communicated with the valve plate, instead, with the housing case. The cylinder block is coupled with the shaft through a spline mechanism and can rotate about the shaft axis along with the drive shaft. The slipper is connected to the piston head via a ball-and-socket joint that can provide three rotational DOFs for the slipper. The compressed cylinder block spring nested within the center bore of the cylinder block serves two functions: firstly, it helps the cylinder block to be held tightly against the valve plate; secondly, it provides a normal force for the retainer so that the slippers can be kept in reasonable contact with the swash plate. The cylinder block bearing is used to support the cylinder block and balance the lateral force arising from the swash-plate reaction force.

When the cylinder block rotates along with the shaft, all pistons reciprocate periodically within piston bores due to the inclined swash plate and retainer. The piston is pulled out from the cylinder block and the fluid flows into the displacement chamber as the piston passes over the intake port. And the piston is pushed into the cylinder block and the fluid flows out of the displacement chamber as the piston passes over the discharge port. During cylinder block rotation, lubricating gaps are formed between the slipper and swash plate, between the piston and cylinder block and between the cylinder block and valve plate.

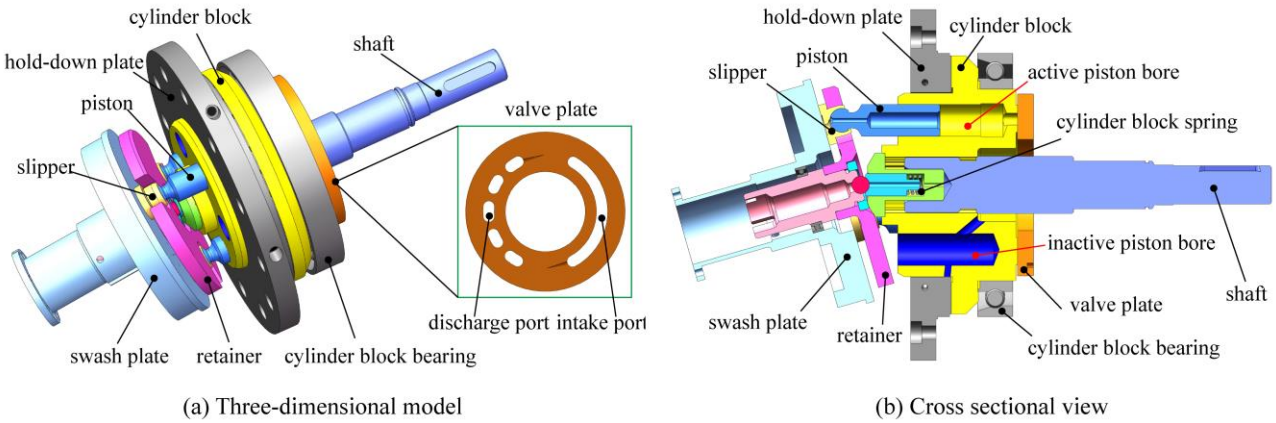

(a) Three-dimensional model (b) Cross sectional view

Fig. 3. Configuration of the three-piston pump

As previously stated, the thin oil film within the three lubricating interfaces has to seal the lubricating gaps and balance the external forces acting on the movable parts such as slipper, piston and cylinder block. Fortunately, the three-piston

pump is redesigned by modifying a commercial axial piston pump. Therefore, for the modified pump, the lubricating gap design of the slipper/swash plate interface and piston/cylinder block interface can be implemented generally based on the experience from the existing commercial pumps. However, the modified pump with a reduced number of pistons probably cannot operate under normal conditions because the fluid force within the cylinder block/valve plate interface is so much larger than the pressing force from the pistons that the cylinder block is pushed away from the valve plate. In addition, a similar problem for the cylinder block occurs in the moment balance.

This work first introduces a hold-down plate to realize the cylinder block balance in the three-piston pump. As illustrated in Fig. 4, the pressurized oil in the hold-down plate is fed from the pump outlet through an oil tube. Then the pressurized oil travels through several oil passages drilled in the hold-down plate into eight identical pockets. The hold-down plate is fixed on the housing case (not shown in Fig. 4) through a set of bolts, ensuring the cylinder block can float between the hold-down plate and valve plate within a reasonable gap height. A hydrostatic pressure distribution is established when the pressurized oil in the pocket flows through the sealing land. It should be noted that the pressure profile across the pocket and sealing land is exaggerated for illustration purpose. The hydrostatic pressure build-up between the hold-down plate and cylinder block creates a fluid force (F_{hyd}) in the Z-axis direction and a fluid moment (M_{hyd}) about the Y-axis. However, there exists no fluid moment coming from hold-down plate about the X-axis due to the fact that these eight identical pockets are distributed symmetrically about the X-axis. The above additional fluid force and moment produced by the hold-down plate are expected to balance the remaining force and moment acting on the cylinder block.

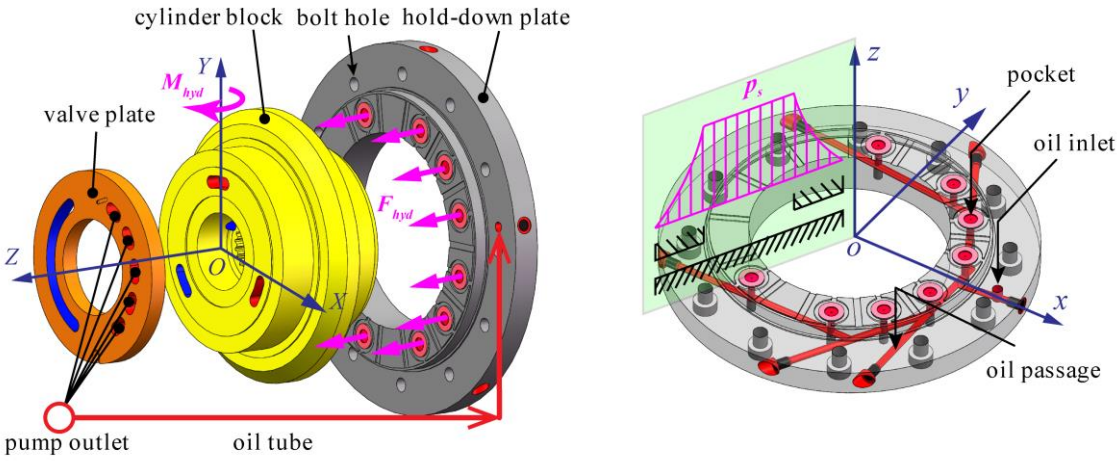

Fig. 4. Working principle of the hold-down plate

3. Mechanical Analysis

Fig. 5 shows the main forces and moments acting on the piston-cylinder block assembly. Specifically, these main forces include the cylinder block spring force (F_{sp}), the swash-plate reaction force (F_N), the cylinder block bearing reaction force (F_b), the fluid force produced by the hold-down plate (F_{hyd}), and the fluid force within the cylinder block/valve plate interface (F_v). In order to simplify the analysis, other forces acting on the piston-cylinder block assembly such as the friction force between the swash plate and slipper, and the inertia force of the piston-slipper assembly are neglected. In Fig. 5, the BDC represents the bottom dead center at which the piston achieves the maximum distance from the cylinder bottom, and the TDC represents the top dead center at which the piston is located at the minimum distance from the cylinder bottom.

Cylinder block spring force and its moment. As previously described, the function of the cylinder block spring is to push the cylinder block towards the fixed valve plate and thus to prevent the cylinder block tilt from the valve plate. The magnitude of the cylinder block spring force is given by [30]

$$F_{sp} \geq \frac{N(m_s + m_p)\omega_{\max}^2 R^2 \tan\beta}{2R_0} \tag{1}$$

where N represents the total number of pistons, m_s and m_p are the mass of a single slipper and piston, respectively, ω_{max} is the maximum angular speed, R is the piston pitch radius, β is the swash-plate angle, and R_0 is the maximum radial dimension of the sealing land on the cylinder block.

The cylinder block spring force will not generate any moments about the origin of the XYZ system because it passes through the origin of the XYZ system.

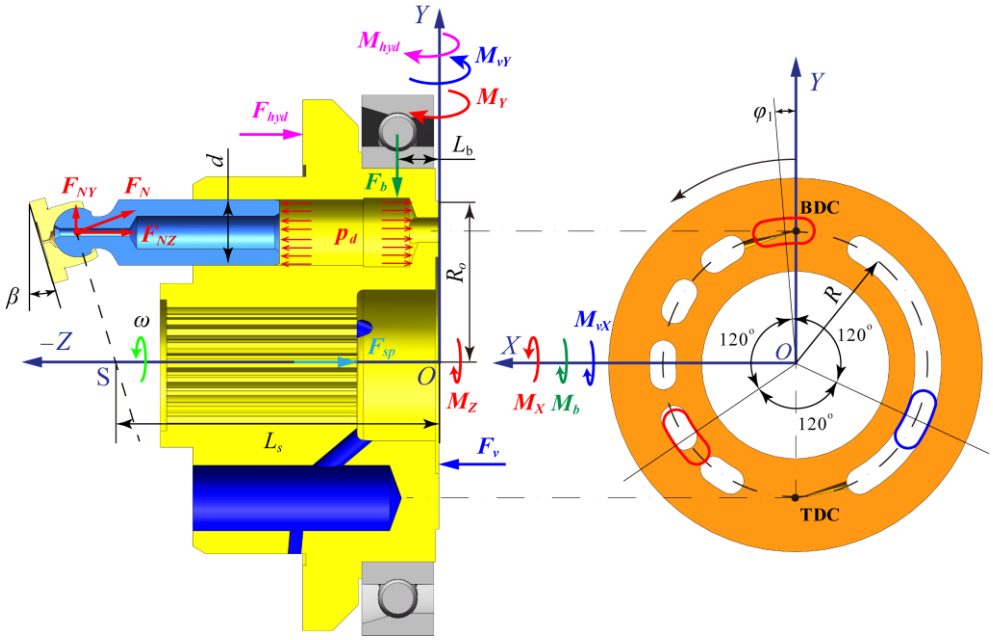

Fig. 5. Forces acting on the piston-cylinder block assembly

Swash-plate reaction force and moment. As shown in Fig. 5, the pressurized fluid in the displacement chamber (p_d) exerts an axial fluid force on the piston-slipper assembly and generates a reaction force on the swash plate. The equations of total force and moment acting on the cylinder block by the swash-plate reaction force can be presented in matrix form:

$$\boldsymbol{F_N} = \begin{pmatrix} F_{NX} \\ F_{NY} \\ F_{NZ} \end{pmatrix} = \frac{1}{4}\pi d^2 \sum_{i=1}^{N} \left[p_{di} \begin{pmatrix} 0 & \tan\beta & 1 \end{pmatrix}^{\mathrm{T}} \right] \tag{2}$$

$$\boldsymbol{M} = \begin{pmatrix} M_X \\ M_Y \\ M_Z \end{pmatrix} = \frac{1}{4}\pi d^2 \sum_{i=1}^{N} \left[p_{di} \begin{pmatrix} L_s \tan\beta + R\sec^2\beta\cos\varphi_i \\ -R\sin\varphi_i \\ R\tan\beta\sin\varphi_i \end{pmatrix} \right] \tag{3}$$

where d is the piston diameter, the lowercase letter i (i=1, 2, 3) denotes the index of the piston, L_s is the distance from the XY plane to the intersection between the shaft axis and the special plane that contains all the piston head centers, and φ_i is the angular position of the ith piston referenced from the first piston.

Cylinder block bearing reaction force and moment. The Y-component of the swash-plate reaction force causes a lateral force that should be balanced by the reaction force of the cylinder block bearing. Thus the cylinder block bearing reaction force may be simply expressed as

$$F_b = -\sum_{i=1}^{N} \frac{1}{4}\pi d^2 p_{di} \tan\beta \tag{4}$$

As shown in Fig. 5, this force can only generate the moment component about the X-axis.

$$M_b = -L_b \sum_{i=1}^{N} \frac{1}{4} \pi d^2 p_{di} \tan \beta \tag{5}$$

where L_b is the moment arm of the cylinder block bearing reaction force.

Displacement chamber pressure. It is observed from Eqs. (2) through (5) that the reaction forces are dependent on the instantaneous displacement chamber pressure. Assuming the fluid in the displacement chamber is compressible, the instantaneous displacement chamber pressure is governed by the following pressure build up equation [31]:

$$\frac{dp_d}{dt} = \frac{K}{V}\left(Q_r - Q_{SS} - Q_{PB} - Q_{BV} - \frac{dV}{dt} \right) \tag{6}$$

where K stands for the bulk modulus of the fluid, which is a function of the temperature and pressure, V is the volume of the displacement chamber, Q_r is the flow into the displacement chamber during motoring mode and out of the displacement chamber during pumping mode, which can be calculated using the standard orifice equation:

$$Q_r = C_d A_H \sqrt{\frac{2|p_d - p_H|}{\rho}} \cdot \mathrm{sgn}(p_d - p_H) + C_d A_L \sqrt{\frac{2|p_d - p_L|}{\rho}} \cdot \mathrm{sgn}(p_d - p_L) \tag{7}$$

where C_d is the orifice coefficient, p_H and p_L are the discharge pressure and intake pressure, respectively, A_H and A_L are the opening area of the discharge port and intake port, respectively, and ρ is the fluid density.

It should be noted that Eq. (7) is a first order, nonlinear differential equation, thus it is not possible to obtain an analytical solution of the pressure profile in the displacement chamber. In addition, this equation includes the leakages through all the lubricating interfaces, which requires an additional gap flow simulation to evaluate their accurate values.

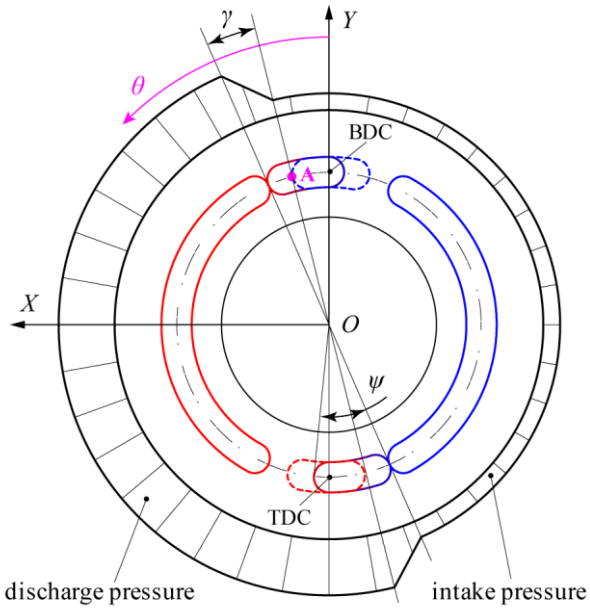

Fig. 6. Pressure profile in the displacement chamber

The schematic method is another way to describe the pressure profile in the displacement chamber, as illustrated in Fig. 6. It becomes more convenient to express the displacement chamber pressure using a simple and discontinuous expression instead of solving the complicated differential equation presented in Eq. (6). Unlike the previous studies [32], the schematic method in this research considers the geometrical size of the kidney-shaped ports in the cylinder block, which makes the calculation of the displacement chamber pressure more accurate in this case. As shown in Fig. 6, the displacement chamber pressure is graphically depicted by the outside profile around the valve plate. The magnitude of pressure changes with the angular position of the point A that is the middle point of the leading edge on the small kidney-shaped port. It is assumed that the displacement chamber pressure remains constant as the small kidney-shaped port passes over the discharge and intake ports. And the displacement chamber pressure is assumed to increase linearly

over the angular distance noted as γ, when the small kidney-shaped port travels from the BDC to the position where the small kidney-shaped port starts to connect itself with the discharge port. Similarly, when the small kidney-shaped port passes over the transition region from the TDC to the intake port, the displacement chamber pressure is assumed to decrease linearly over the angular distance of γ.

Thus, the displacement chamber pressure as a function of the angular position of the point A may be written as

$$p_d(\theta)=\begin{cases} p_L+(\theta-\psi/2)\dfrac{p_H-p_L}{\gamma} & \psi/2<\theta\le\psi/2+\gamma \\ p_H & \psi/2+\gamma<\theta\le\pi+\psi/2 \\ p_H-\left[\theta-(\pi+\psi/2)\right]\dfrac{p_H-p_L}{\gamma} & \pi+\psi/2<\theta\le\pi+\psi/2+\gamma \\ p_L & \pi+\psi/2+\gamma<\theta\le 2\pi+\psi/2 \end{cases} \tag{8}$$

where θ is the angular position of the point A, and ψ represents the angular span of the small kidney-shaped port in the cylinder block.

Substituting $\theta=\varphi+\psi/2$ into Eq. (8) yields the expression for the displacement chamber pressure as a function of the angular position of the piston.

$$p_d(\varphi)=\begin{cases} p_L+\varphi\dfrac{p_H-p_L}{\gamma} & 0<\varphi\le\gamma \\ p_H & \gamma<\varphi\le\pi \\ p_H-(\varphi-\pi)\dfrac{p_H-p_L}{\gamma} & \pi<\varphi\le\pi+\gamma \\ p_L & \pi+\gamma<\varphi\le 2\pi \end{cases} \tag{9}$$

Fluid force and moment from the hold-down plate. As shown in Fig. 7, the pockets in the hold-down plate are distributed symmetrically around the *X*-axis. Assuming the pump case pressure is zero, the total fluid force coming from these eight pockets acting on the cylinder block in the *Z*-axis direction may be given by

$$\sum F_{hyd}=\zeta 4\pi p_H\frac{r_2^2-r_1^2}{\ln r_2-\ln r_1} \tag{10}$$

where r_1 is the inner radius of the sealing land, r_2 is the outer radius of the sealing land, ζ is the pressure-loss coefficient considering there exist pressure losses as the pressurized oil flows through the pump outlet to the pockets.

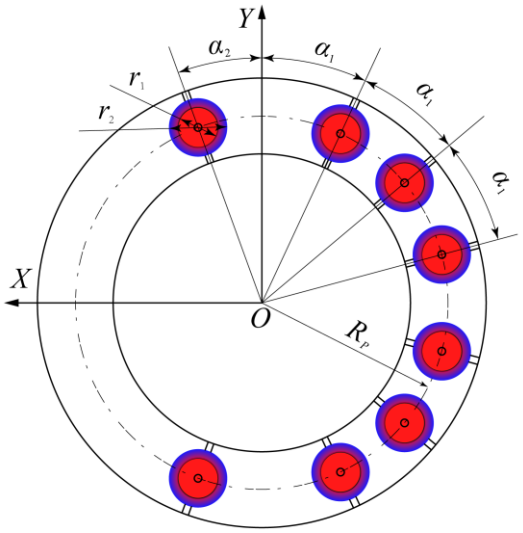

Fig. 7. Pockets location on the hold-down plate

Due to the symmetric distribution of the pockets about the *X*-axis, the fluid force of the hold-down plate only generates moment on the cylinder block about the *Y*-axis. The moment acting on the cylinder block by the hold-down device can be expressed as

$$\sum M_{hyd} = -\zeta \pi p_H \frac{r_2^2 - r_1^2}{\ln r_2 - \ln r_1} R_P \left(\sin\alpha_1 + \sin 2\alpha_1 + \sin 3\alpha_1 - \sin\alpha_2 \right) \tag{11}$$

where the dimensions R_P, α_1, and α_2 determine the location of each pocket in the hold-down plate, as seen in Fig. 7.

Fluid force and moment within the cylinder block/valve plate interface. Fig. 8 shows the main geometric dimensions of the cylinder block/valve plate interface, which will be involved in the following calculations of the fluid force and moment. Assuming the pump case pressure is zero, the pressure across the sealing land and kidney on the discharge side is given as [32]

$$p = \begin{cases} p_H \dfrac{\ln r - \ln R_1}{\ln R_2 - \ln R_1} & R_1 \le r \le R_2 \\ p_H & R_2 \le r \le R_3 \\ p_H \dfrac{\ln R_4 - \ln r}{\ln R_4 - \ln R_3} & R_3 \le r \le R_4 \end{cases} \tag{12}$$

where R_1, R_2, R_3, and R_4 are the radii dimensions of the sealing land within the cylinder block/valve plate interface.

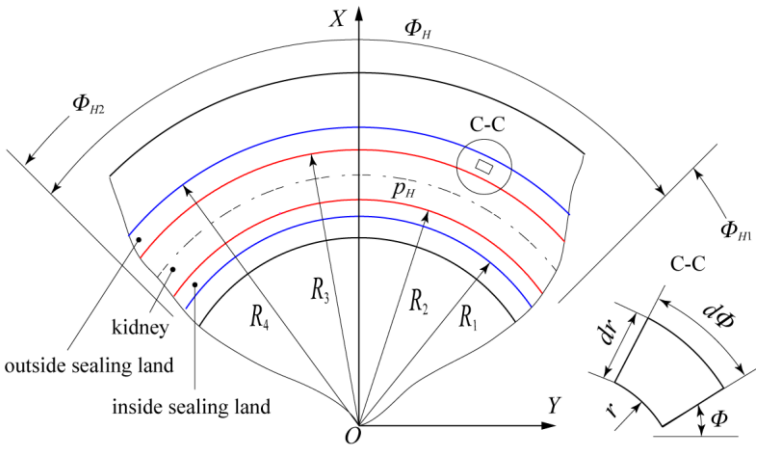

Fig. 8. Main geometric dimensions of the cylinder block/valve plate interface

By integrating Eq. (12) over the entire pressurized area, the fluid forces generated on the discharge side and intake side within the cylinder block/valve plate interface can be given by

$$F_{vH} = -\int_{\Phi_{H1}}^{\Phi_{H2}} \left(\int_{R_1}^{R_2} p_H \frac{\ln r - \ln R_1}{\ln R_2 - \ln R_1} r dr + \int_{R_2}^{R_3} p_H r dr + \int_{R_4}^{R_4} p_H \frac{\ln R_4 - \ln r}{\ln R_4 - \ln R_3} r dr \right) d\Phi \tag{13}$$

$$F_{vL} = -\int_{\Phi_{L1}}^{\Phi_{L2}} \left(\int_{R_1}^{R_2} p_L \frac{\ln r - \ln R_1}{\ln R_2 - \ln R_1} r dr + \int_{R_2}^{R_3} p_L r dr + \int_{R_4}^{R_4} p_L \frac{\ln R_4 - \ln r}{\ln R_4 - \ln R_3} r dr \right) d\Phi \tag{14}$$

where Φ_{H1} and Φ_{H2} are the starting and ending angles of the effective discharge area, respectively, Φ_{L1} and Φ_{L2} are the starting and ending angles of the effective intake area. These four angles are determined by the angular position of the small kidney-shaped port in the cylinder block with respect to the discharge port in the valve plate.

The resulting fluid force acting on the cylinder block is the sum of the fluid forces presented in Eqs. (13) and (14). Substituting Eq. (12) into Eqs. (13) and (14), and considering $\Phi_H = \Phi_{H2} - \Phi_{H1}$ and $\Phi_L = \Phi_{L2} - \Phi_{L1}$, the above resulting fluid force is given by

$$F_v = -\frac{1}{4}\left(\Phi_H p_H + \Phi_L p_L\right)\left(\frac{R_4^2 - R_3^2}{\ln R_4 - \ln R_3} - \frac{R_2^2 - R_1^2}{\ln R_2 - \ln R_1}\right) \tag{15}$$

where Φ_H and Φ_L are the effective angular spans of the discharge area and intake area, respectively.

By integrating Eq. (12) over the entire pressurized area, the fluid moments about the *X*-axis generated on the discharge side and intake side are

$$M_{vHX} = -\int_{\Phi_{H1}}^{\Phi_{H2}}\left(\int_{R_1}^{R_2} p_H \frac{\ln r - \ln R_1}{\ln R_2 - \ln R_1} r^2 \cos\Phi dr + \int_{R_2}^{R_3} p_H r^2 \cos\Phi dr + \int_{R_3}^{R_4} p_H \frac{\ln R_4 - \ln r}{\ln R_4 - \ln R_3} r^2 \cos\Phi dr\right) d\Phi \tag{16}$$

$$M_{vLX} = -\int_{\Phi_{L1}}^{\Phi_{L2}}\left(\int_{R_1}^{R_2} p_L \frac{\ln r - \ln R_1}{\ln R_2 - \ln R_1} r^2 \cos\Phi dr + \int_{R_2}^{R_3} p_L r^2 \cos\Phi dr + \int_{R_3}^{R_4} p_L \frac{\ln R_4 - \ln r}{\ln R_4 - \ln R_3} r^2 \cos\Phi dr\right) d\Phi \tag{17}$$

Therefore, the resulting fluid moment about the *X*-axis is the sum of the fluid moments from the discharge side and intake side.

$$M_{vX} = -\frac{1}{9}\left(\frac{R_4^3 - R_3^3}{\ln R_4 - \ln R_3} - \frac{R_2^3 - R_1^3}{\ln R_2 - \ln R_1}\right)\left[\left(\sin\Phi_{H2} - \sin\Phi_{H1}\right) p_H + \left(\sin\Phi_{L2} - \sin\Phi_{L1}\right) p_L\right] \tag{18}$$

Similarly, the resulting fluid moment about the *Y*-axis within the cylinder block/valve plate interface is

$$M_{vY} = -\frac{1}{9}\left(\frac{R_4^3 - R_3^3}{\ln R_4 - \ln R_3} - \frac{R_2^3 - R_1^3}{\ln R_2 - \ln R_1}\right)\left[\left(\cos\Phi_{H2} - \cos\Phi_{H1}\right) p_H + \left(\cos\Phi_{L2} - \cos\Phi_{L1}\right) p_L\right] \tag{19}$$

The fluid force and moments presented in Eqs. (15), (18), and (19) are highly dependent on the pressure distribution area within the cylinder block/valve plate interface. Comparing with commercial axial piston pumps, the effective angular spans of the discharge area and intake area in this three-piston pump change more remarkably during cylinder block rotation due to the reduced number of pistons. Therefore, it is necessary to accurately evaluate the effective angular spans of the discharge area and intake area when calculating the fluid force and moments within the cylinder block/valve plate interface.

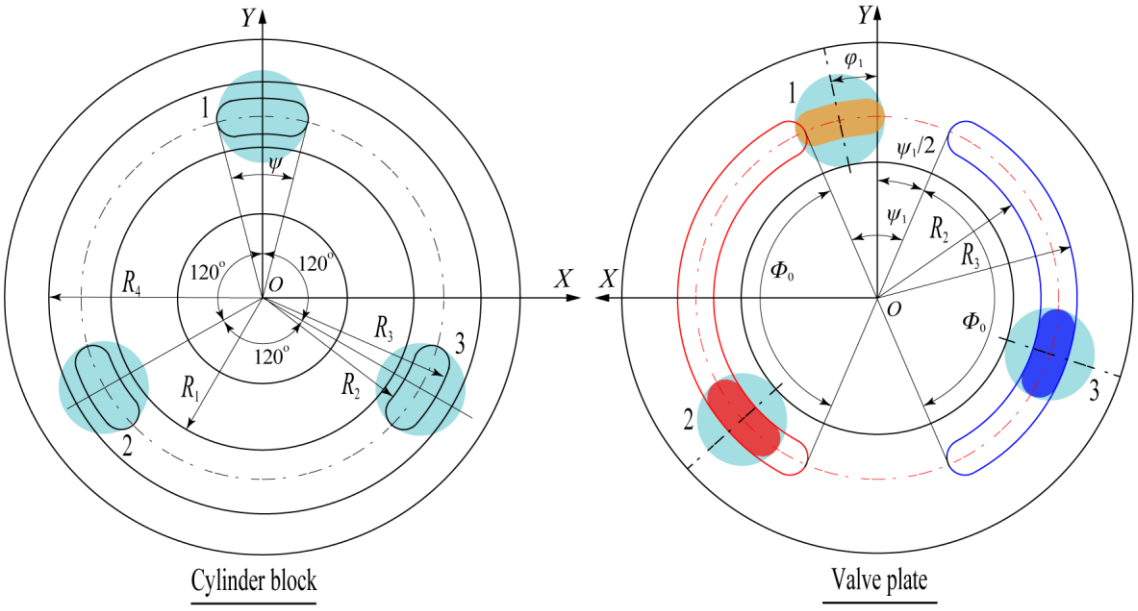

Fig. 9. Contact interface between cylinder block and valve plate

As shown in Fig. 9, the effective angular spans of the discharge area and intake area vary as the kidney-shaped ports in the cylinder block pass over both ports in the valve plate. It is assumed that the effective angular span of either the

discharge area or the intake area equals to the original angular span (Φ_0) if no kidney-shaped ports in the cylinder block are connected to the two ports in the valve plate. However, if any kidney-shaped port in the cylinder block is communicated with the discharge port or intake port, then the effective angular spans of the discharge area and intake area must take into account the angular span of the small kidney-shaped port.

Fig. 10 gives the critical angular positions of the cylinder block during rotation. It can be observed from Fig. 10 that the effective angular span of either discharge area or intake area starts to change when one of small kidney-shaped ports is exactly touching or leaving the discharge port and intake port in the valve plate. The effective angular spans of discharge area and intake area may be expressed in terms of the first piston's angular displacement φ_1.

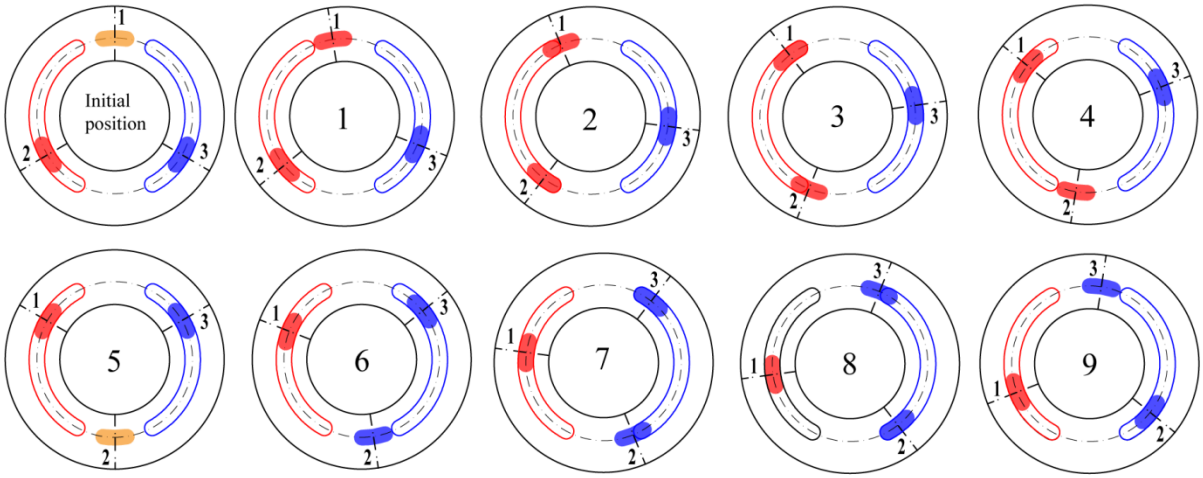

Fig. 10. Critical angular positions of the cylinder block relative to the valve plate

$$\begin{cases} \Phi_{H1} = \psi_1/2 \\ \Phi_{H2} = \psi_1/2 + \Phi_0 \\ \Phi_{L1} = 2\pi - (\psi_1/2 + \Phi_0) \\ \Phi_{L2} = 2\pi - \psi_1/2 \end{cases} \quad 0 \le \varphi_1 \le (\psi_1 - \psi)/2 \tag{20}$$

$$\begin{cases} \Phi_{H1} = \varphi_1 - \psi/2 \\ \Phi_{H2} = \psi_1/2 + \Phi_0 \\ \Phi_{L1} = 2\pi - (\psi_1/2 + \Phi_0) \\ \Phi_{L2} = 2\pi - \psi_1/2 \end{cases} \quad (\psi_1 - \psi)/2 < \varphi_1 \le (\psi_1 - \psi)/2 + \Phi_0 - 2\pi/3 \tag{21}$$

$$\begin{cases} \Phi_{H1} = \varphi_1 - \psi/2 \\ \Phi_{H2} = \varphi_1 + \psi/2 + 2\pi/3 \\ \Phi_{L1} = 2\pi - (\psi_1/2 + \Phi_0) \\ \Phi_{L2} = 2\pi - \psi_1/2 \end{cases} \quad (\psi_1 - \psi)/2 + \Phi_0 - 2\pi/3 < \varphi_1 \le (\psi_1 + \psi)/2 \tag{22}$$

$$\begin{cases} \Phi_{H1} = \psi_1/2 \\ \Phi_{H2} = \varphi_1 + \psi/2 + 2\pi/3 \\ \Phi_{L1} = 2\pi - (\psi_1/2 + \Phi_0) \\ \Phi_{L2} = 2\pi - \psi_1/2 \end{cases} \quad (\psi_1 + \psi)/2 < \varphi_1 \le (\psi_1 + \psi)/2 + \Phi_0 - 2\pi/3 \tag{23}$$

$$\begin{cases} \Phi_{H1} = \psi_1/2 \\ \Phi_{H2} = \psi_1/2 + \Phi_0 \\ \Phi_{L1} = 2\pi - (\psi_1/2 + \Phi_0) \\ \Phi_{L2} = 2\pi - \psi_1/2 \end{cases} \quad (\psi_1 + \psi)/2 + \Phi_0 - 2\pi/3 < \varphi_1 \le \Phi_0 - 2\pi/3 + 3\psi_1/2 - \psi/2 \tag{24}$$

$$\begin{cases} \Phi_{H1} = \psi_1/2 \\ \Phi_{H2} = \psi_1/2 + \Phi_0 \\ \Phi_{L1} = \varphi_1 + 2\pi/3 - \psi/2 \\ \Phi_{L2} = 2\pi - \psi_1/2 \end{cases} \quad \Phi_0 - 2\pi/3 + 3\psi_1/2 - \psi/2 < \varphi_1 \le 2\pi/3 - (\psi + \psi_1)/2 \tag{25}$$

$$\begin{cases} \Phi_{H1} = \psi_1/2 \\ \Phi_{H2} = \psi_1/2 + \Phi_0 \\ \Phi_{L1} = \varphi_1 + 2\pi/3 - \psi/2 \\ \Phi_{L2} = \varphi_1 + 4\pi/3 + \psi/2 \end{cases} \quad 2\pi/3 - (\psi + \psi_1)/2 < \varphi_1 \le 4\pi/3 - (\psi_1 - \psi)/2 - \Phi_0 \tag{26}$$

$$\begin{cases} \Phi_{H1} = \psi_1/2 \\ \Phi_{H2} = \psi_1/2 + \Phi_0 \\ \Phi_{L1} = 2\pi - (\psi_1/2 + \Phi_0) \\ \Phi_{L2} = \varphi_1 + 4\pi/3 + \psi/2 \end{cases} \quad 4\pi/3 - (\psi_1 - \psi)/2 - \Phi_0 < \varphi_1 \le 2\pi/3 - (\psi_1 - \psi)/2 \tag{27}$$

$$\begin{cases} \Phi_{H1} = \psi_1/2 \\ \Phi_{H2} = \psi_1/2 + \Phi_0 \\ \Phi_{L1} = 2\pi - (\psi_1/2 + \Phi_0) \\ \Phi_{L2} = 2\pi - \psi_1/2 \end{cases} \quad 2\pi/3 - (\psi_1 - \psi)/2 < \varphi_1 \le 2\pi/3 \tag{28}$$

where ψ_1 is the angular distance between the discharge port and intake port, as shown in Fig. 9.

4. Balance factor of the cylinder block

The three-piston pump is more likely to suffer from imbalance between the external forces and fluid forces when comparing with commercial piston pumps. Therefore, the cylinder block balance is a key issue of the three-piston pump design. In this research, the hydrodynamic forces for the cylinder block are not calculated for modeling expediency, but the hydrodynamic effect will be considered in the balance ratios of the cylinder block. The balance ratio of force for the cylinder block is defined as the ratio of the fluid force within the cylinder block/valve plate interface to the external force in the *Z*-axis direction.

$$B_Z = \left| \frac{F_v}{F_{sp} + F_{NZ} + \sum F_{hyd}} \right| \tag{29}$$

Similarly, the balance ratio of moment for the cylinder block is defined as the ratio of the fluid moment to the external moment about the *Y*-axis.

$$B_Y = \left| \frac{M_{vY}}{M_Y + \sum M_{hyd}} \right| \tag{30}$$

Typically, a reasonable balance ratio is usually between 0.9 and 1 [33]. The balance ratio of moment about the *X*-axis is not defined here because, unlike the moments about the *Y*-axis, the moments about the *X*-axis frequently change their directions. In practice, it is hoped that the mean value of resultant moments in the *X*-axis direction is adjacent to zero. Therefore, the remaining moment about the *X*-axis is used to evaluate the cylinder block balance about the *X*-axis.

$$B_X = M_{vX} + M_X + M_b \tag{31}$$

Table 1

Three-piston pump parameters

Parameter	Value	Parameter	Value
Angular dimensions of pockets α_1, α_2 (deg)	25, 20	Distance of point S from XY plane L_s (mm)	99.5
Swash plate angle β (deg)	5	Moment arm L_b (mm)	11
Angular distance of pressure transition γ (deg)	9.1	Piston pitch radius R (mm)	40.5
Original angular span of ports Φ_0 (deg)	133.4	Radius of sealing land of pocket r_1, r_2 (mm)	5, 7.5
Angular span of small kidney-shaped port ψ (deg)	28.4	Pocket pitch radius R_P (mm)	70
Angular distance between two ports ψ_1 (deg)	46.6	Radial dimensions of sealing land R_1 (mm)	33.35
Pressure-loss coefficient ζ	0.9	Radial dimensions of sealing land R_2 (mm)	36.5
Piston diameter d (mm)	20	Radial dimensions of sealing land R_3 (mm)	44.5
Cylinder block spring force F_{sp} (N)	411	Radial dimensions of sealing land R_4 (mm)	49.75

Table 1 gives the main three-piston pump parameters that are used to calculate the balance ratios for the cylinder block. As previous stated, the balance ratios for the cylinder block must be in a reasonable range, otherwise excessive balance ratios will result in the cylinder block separating from the valve plate. Fig. 11 shows the comparison of balance ratios of force with and without the hold-down plate, which indicates that the proposed hold-down plate can effectively adjust the balance ratio of force to a reasonable value between 0.9 and 1. The mean value of the balance ratio of force without the hold-down plate is 2.68, while it becomes 0.92 after using the hold-down plate. Similarly, the balance ratio of moment about the Y-axis is adjusted to a reasonable value successfully, as shown in Fig. 12. The mean values of balance ratio of moment with and without the hold-down plate are 0.95 and 3.19, respectively.

The last important design criteria for the cylinder block balance is the remaining moment about the X-axis. As shown in Fig. 13, the magnitude of this remaining moment changes between positive and negative values, and its mean value is 59.85 N·m in a cycle. Generally, the mean value of the remaining moment is desired to be near zero because a smaller mean value means a better cylinder block balance about the X-axis. Unfortunately, the remaining moment of 59.85 N·m will cause the cylinder block to tilt slightly towards the BDC and thus give rise to more wear in this region. Increasing the moment arm of the cylinder block bearing reaction force is a possible way to reduce this potential wear. For instance, the mean value of the remaining moment can be reduced to 34.45 N·m if the moment arm is 5 times the length of the original one. Furthermore, if the moment arm is 10 times the length of the original one, the remaining moment is only 2.71 N·m. However, the cylinder block bearing is still chosen to be mounted at its current location rather than other locations where can provide a longer moment arm. This is mainly because there is not enough space to mount the cylinder block bearing for a longer moment arm due to the existence of the hold-down plate.

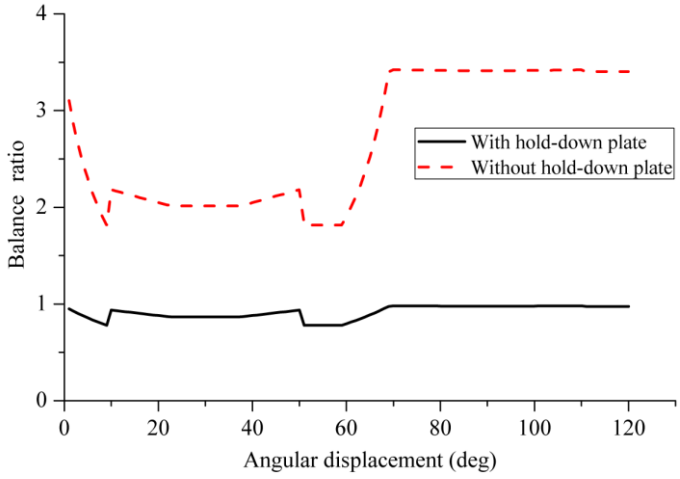

Fig. 11. Comparison of balance ratio of force in the Z-axis direction (p_L = 0.5 MPa, p_H = 20 MPa)

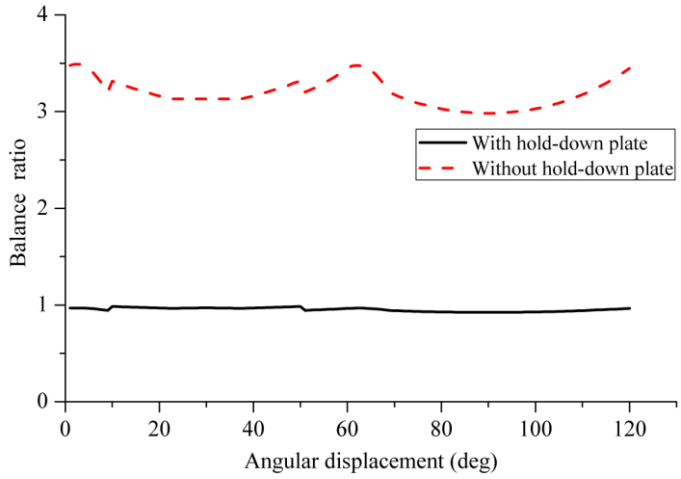

Fig. 12. Comparison of balance ratio of moment about the *Y*-axis (p_L = 0.5 MPa, p_H = 20 MPa)

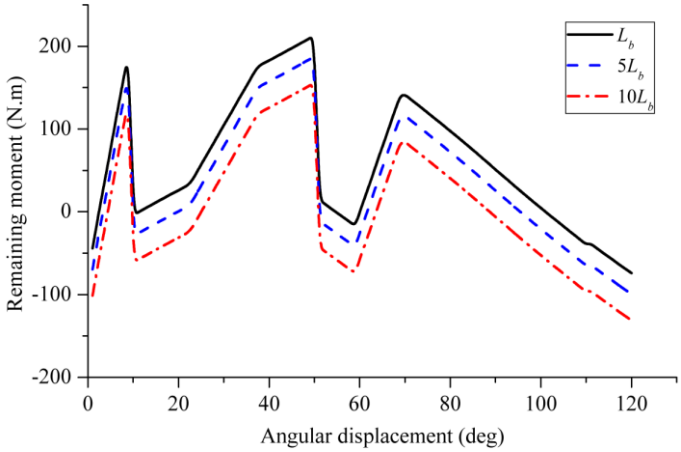

Fig. 13. Remaining moment about the *X*-axis (p_L = 0.5 MPa, p_H = 20 MPa)

5. Experiments

It is commonly known that the sensors are not easy to install in the limited space available in commercial axial piston pumps for continuous measurements of the slipper bearing parameters. The slipper test rig benefited from this three-piston pump since the reduced number of pistons could bring enough space for sensor installation. As a practical application of this three-piston pump, the slipper spin measurement was carried out on it. As shown in Fig. 14, the slipper slid on the swash plate in an elliptical path [18]. If the slipper's spinning motion occurred, then the slipper would rotate about its own axis when sliding on the swash plate. In order to continuously measure the spinning speed of the slipper, the retainer was selected to mount the displacement sensor so that the sensor could follow the sliding target slipper, as shown in Fig. 15.

There were totally three different slippers within this three-piston pump. The drive slipper was responsible for driving the modified retainer that was supported by a ball bearing. The drive slipper's corresponding U-shaped slot was designed to be tangential to the slipper's neck surface, so that it could allow a simultaneous motion of the slipper and modified retainer. The auxiliary slipper was used to improve the stability of the cylinder block since the cylinder block balance could benefit from more pistons. The test slipper played an important role in the slipper spin measurement. Unlike the drive slipper, its corresponding U-shaped slot was designed to be slightly bigger than its neck, so that the catastrophic contact between the sensor and the test slipper could be avoided. There were several machined grooves evenly distributed on the neck surface of the test slipper. An eddy current displacement sensor (KD-2446) was fixed in the modified retainer by a thread machined on the wing-shaped plate. The sensor face was close to the test slipper to capture its spinning behavior. Once the slipper spin took place, the grooves on the test slipper neck would pass the sensor and thus caused an increase in the sensor output voltage. The sensor output signals were transmitted from the moving modified retainer to

the stationary recorder by a slip ring. Using this principle, the slipper spin could be detected and the spinning speed might be obtained by counting the instantaneous voltage increase from the sensor. Table 2 lists the details of the used eddy current displacement sensor.

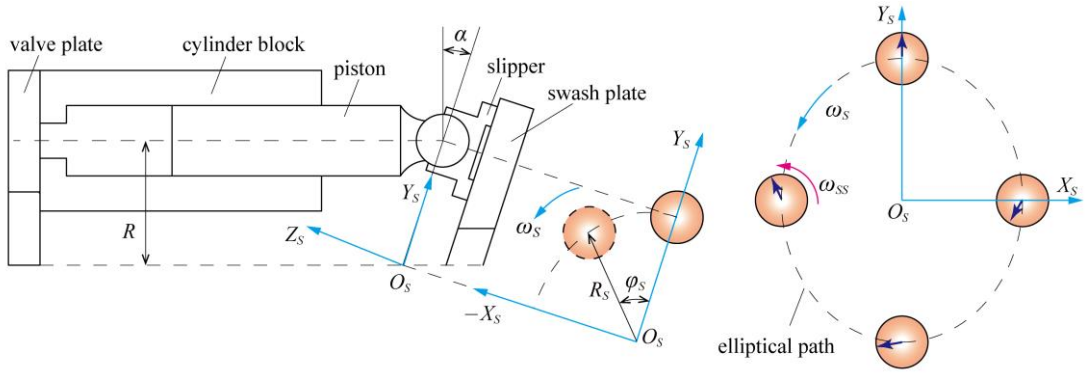

Fig. 14. Schematic of the slipper motion on the swash plate

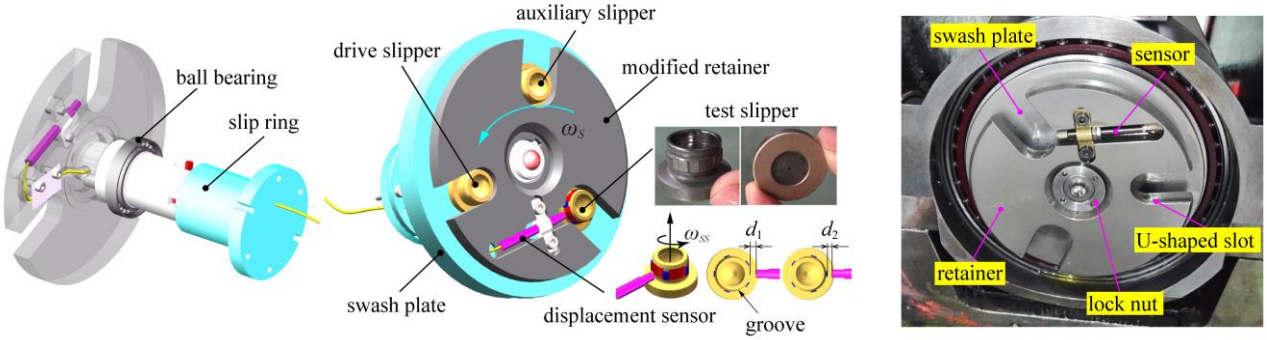

Fig. 15. Slipper spin measurement using an displacement sensor

Table 2

Details of the eddy current displacement sensor (KD-2446)

Description	Value	Description	Value
Diameter of sensor face	4.1 mm	Voltage input	12-24 V
Measuring range	0.38-3.81 mm	Resolution	⩽0.008% of measuring range
Temperature range	–52 °C-205 °C	Temperature shift	⩽0.22% per °C of full scale
Frequency response	0-10 KHz (± 3db)		

In order to measure the slipper's spinning motion, a slipper test rig was built, as shown in Fig. 16. The test rig mainly included the three-piston pump, drive motor, control system, and data logging system. The test pump was driven by the motor using a coupling. Like a commercial axial piston pump, the test pump could accomplish the basic task of displacing working fluid for each revolution along with the drive motor. The charge pump was used to compensate for the inadequate inlet pressure of the test pump, and the inlet pressure was regulated by a pressure relief valve. Similarly, the pressure relief valve in the outlet line of the test pump was used to adjust the pump discharge pressure. As previously stated, the discharge pressure of the test pump was introduced to the hold-down plate to produce an additional hydraulic pressing force for the cylinder block. All signals obtained from the sensors were collected by a group of NI DAQ modules. In addition, a Labview program was employed to monitor and record the measured data. The voltage signals from the eddy current displacement sensor started to be collected after the test pump worked for several minutes and reached a relatively steady state.

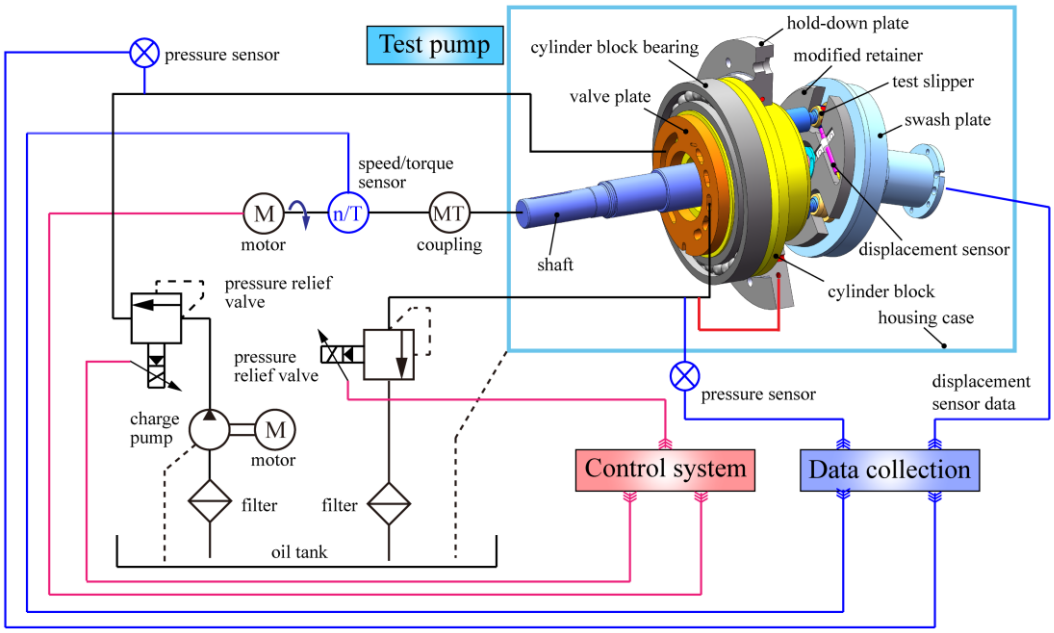

Fig. 16. Schematic of the slipper test rig for slipper spin measurement

Fig. 17 shows an example of the output voltage from the eddy current displacement sensor for two shaft revolutions. Note that the voltage magnitude has been normalized by its baseline value at the beginning of measurement. It can be observed from Fig. 17 that the magnitude of the output voltage varies with the shaft angular displacement, which indicates that the eddy current displacement sensor is able to capture the displacement variation of the slipper within this three-piston pump. The displacement variation mainly results from the slipper's macro motion (i.e., the translational motion in elliptical manner) on the swash plate. Additionally, some local voltage increases are found to be superimposed on the main voltage curve. This may be explained by the fact that the slipper spin takes place, and the grooves on the test slipper neck are detected by the eddy current displacement sensor. It has to be pointed out that some possible factors regarding the measuring error may be involved during measurements, for example, the undesirable vibration of the hydraulic system and non-linear relationship between the sensor output and the measured distance.

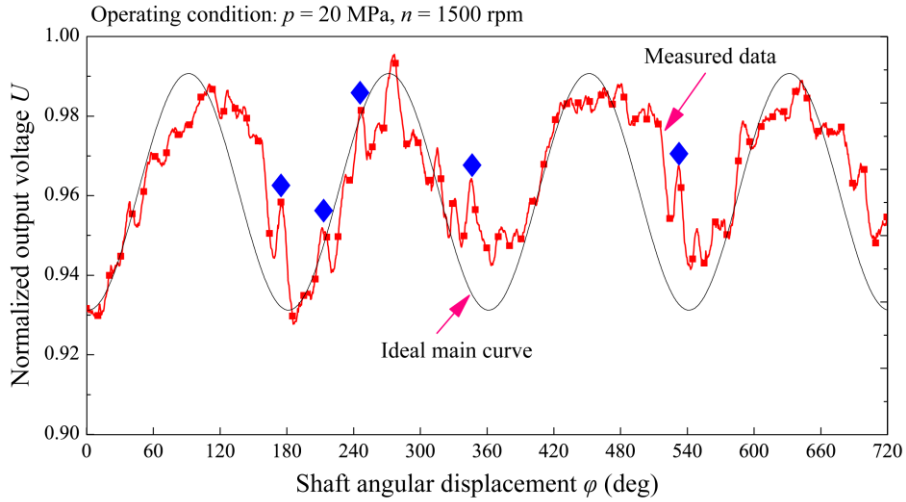

Fig. 17. Measured results of output voltage for the eddy current displacement sensor

It was worth pointing out that the original design of this three-piston pump did not include the hold-down plate. As a result, the cylinder block was pushed away from the valve plate, and a large amount of leakage across the cylinder block/valve plate interface did not allow the test pump to operate at more than 2 MPa. However, the maximum pressure

of the test pump could reach 20 MPa and the maximum speed 1500 rpm after including the hold-down plate. The three-piston pump was disassembled to examine the contact surfaces after experiments, as shown in Fig. 18. More attentions are paid to the contact surfaces between the hold-down plate and cylinder block, and between the cylinder block and valve plate, since these two contact surfaces are most likely to suffer from metal-to-metal contact. It can be observed from Fig. 18 that the contact surface between the hold-down plate and cylinder block do not suffer from obvious wear, which gives confidence to the method of hold-down plate for the three-piston pump.

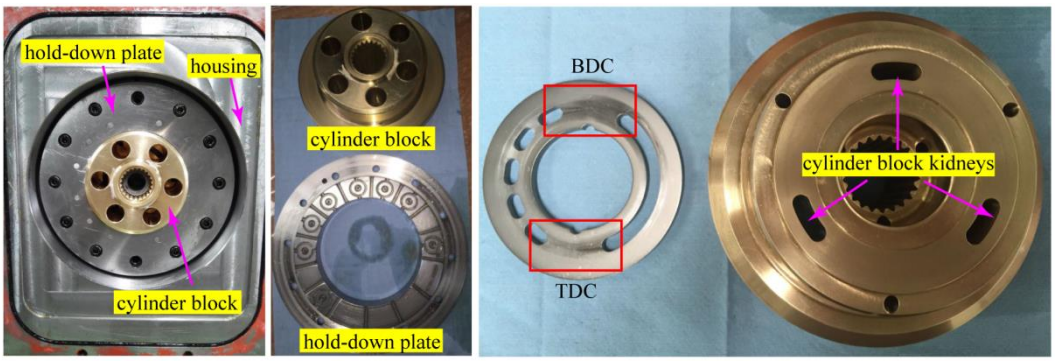

Fig. 18. Photographic view of the cylinder block, hold-down plate, and valve plate after experiments

6. Discussion and conclusion

This paper has proposed a novel three-piston pump for a slipper test rig. The reduced number of pistons helps to address the potential space limitation of the sensor installation, and the special hold-down plate makes it possible for the three-piston pump to overcome the drawback of the cylinder block imbalance. The three-piston pump was redesigned based on a commercial axial piston pump and minimized alterations to the original pump components, which makes it easy for the test pump to disassemble for refurbishing or remanufacturing. Also, the three-piston pump can fulfill both the real kinematics behavior of slippers and the flow communication between the cylinder and valve plate. This is helpful to remain the measurement integrity for the slipper test rig. The slipper spin measurement carried out on the slipper test rig confirms the reliability of the three-piston pump. Although the three-piston pump has been proved to be applicable in the slipper test rig, there is still a strong need to improve the test pump performance in the following aspects.

Firstly, the valve plate has obvious wear at the region of the BDC since the remaining moment acting on the cylinder block about the *X*-axis makes the cylinder block slightly tilt towards the BDC. As a result, a potential metal-to-metal contact between the cylinder block and valve plate takes place. A possible solution is to mount the cylinder block bearing near the swash plate for a longer moment arm of the reaction force, but this requires the pump configuration to be rearranged so that it can provide enough space to mount the cylinder block bearing.

Secondly, the reduced number of pistons will adversely affect the outflow of the test pump, resulting in a relatively large flow pulsation, and thus an increase in the fluid-borne noise. On the one hand, considering the original commercial pump has nine pistons, the test pump may still provide enough space for the sensor installation after careful modification even though the number of pistons is seven or five. Thus there is still some room for improvement in the flow pulsation by increasing the number of pistons. On the other hand, the flow pulsation has a strong relationship with the displacement chamber pressure which is highly influenced by the valve plate design. Therefore, the reduction of the flow pulsation can also benefit from the valve plate optimization, especially the relief groove optimization.

Thirdly, the displacement sensor is installed in the retainer and rotates along with the retainer over the swash plate. The output signals from the sensor have to be transmitted from the rotating retainer to the stationary recorder by a slip ring. The test pump cannot operate at very high speeds because of the mass eccentricity of the modified retainer containing the sensor. The another reason for the limitation of the pump speed is that the centrifugal force and viscous force acting on the sensor cable attempt to separate it from the modified retainer when it rotates along with the retainer in the oil-filled housing case.

Future experimental research on the slipper will take advantage of the full capacity of the three-piston pump. For example, it is possible to experimentally investigate the oil-film parameters of the slipper bearing, such as oil-film thickness, pressure, and temperature. In addition, possible future research topics can be the extension to the

piston/cylinder block interface because the reduced number of pistons also contributes to providing additional space for the sensor installation on the cylinder block.

Funding

The authors would like to appreciate the financial support received from National Basic Research Program of China (973 Program) (No. 2014CB046403) and National Natural Science Foundation of China (No. 51475462).

References

[1] H.Y. Yang, M. Pan, Engineering research in fluid power: a review, Journal of Zhejiang University SCIENCE A 16(6) (2015) 427-442.

[2] N. Iboshi, A. Yamaguchi, Characteristics of a slipper bearing for swash plate type axial piston pumps and motors (1st report, Theoretical analysis), Bulletin of JSME 25(210) (1982) 1921-1930.

[3] N. Iboshi, A. Yamaguchi, Characteristics of a slipper bearing for swash plate type axial piston pumps and motors (2nd report, Experiment), Bulletin of JSME 26 (219) (1983) 1583–1589.

[4] H. Yabe, A. Kubo, Fundamental characteristics of slipper bearings in swash plate type axial piston pumps and motors (1st report, Fundamental bearing characteristics), Transactions of the Japan Society of Mechanical Engineers Part C 63(608) (1997) 1350-1356.

[5] K. Tanaka, T. Nakahara, K. Kyogoku, K. Fujita, Motion characteristics of slipper bearing in swash plate type piston pump and motor, Transactions of the Japan Society of Mechanical Engineers Part C 19(4) (2007) 1236-1244.

[6] M. Borghi, E. Specchia, B. Zardin, Numerical analysis of the dynamic behaviour of axial piston pumps and motors slipper bearings, SAE International Journal of Passenger Cars-Mechanical Systems 2(2009-01-1820) (2009) 1285-1302.

[7] S. Lin, J.B. Hu, Tribo-dynamic model of slipper bearings, Applied Mathematical Modelling 39(2) (2015) 548-558.

[8] R.M. Harris, K.A. Edge, D.G. Tilley, Predicting the behavior of slipper pads in swashplate-type axial piston pumps, Journal of Dynamic Systems, Measurement, and Control 118(1) (1996) 41-47.

[9] N.D. Manring, Slipper tipping within an axial-piston swash-plate type hydrostatic pump, in: ASME International Mechanical Engineering Congress and Exposition, Anaheim, California, USA, November 15–20, 1998, pp. 169-175.

[10] M. Borghi, E. Specchia, B. Zardin, E. Corradini, The critical speed of slipper bearings in axial piston swash plate type pumps and motors, in: ASME 2009 Dynamic Systems and Control Conference, Hollywood, California, USA, October 12-14, 2009, pp. 267-274.

[11] C.J. Hooke, Y.P. Kakoullis, The effects of non-flatness on the performance of slippers in axial piston pumps, Proceedings of the Institution of Mechanical Engineers, Part C: Journal of Mechanical Engineering Science 197(4) (1983) 239-247.

[12] C.J. Hooke, K.Y. Li, The lubrication of overclamped slippers in axial piston pumps—centrally loaded behaviour, Proceedings of the Institution of Mechanical Engineers, Part C: Journal of Mechanical Engineering Science 202(4) (1988) 287-293.

[13] C.J. Hooke, K.Y. Li, The lubrication of slippers in axial piston pumps and motors—the effect of tilting couples. Proceedings of the Institution of Mechanical Engineers, Part C: Journal of Mechanical Engineering Science 203(5) (1989) 343-350.

[14] B. Xu, J.H. Zhang, H.Y. Yang, Investigation on structural optimization of anti-overturning slipper of axial piston pump, Science China Technological Sciences 55(11) (2012) 3010-3018.

[15] Y.H. Li, Z.L. Ji, L.M. Yang, P. Zhang, B. Xu, J.H. Zhang, Thermal-fluid-structure coupling analysis for valve plate friction pair of axial piston pump in electrohydrostatic actuator (EHA) of aircraft, Applied Mathematical Modelling (2016), doi: http://dx.doi.org/10.1016/j.apm.2016.08.015.

[16] U. Wieczorek, M. Ivantysynova, Computer aided optimization of bearing and sealing gaps in hydrostatic machines—the simulation tool CASPAR, International Journal of Fluid Power 3(1) (2002) 7-20.

[17] C.C. Huang, CASPAR based slipper performance prediction in axial piston pumps, in: 3rd FPNI-PhD Symposium on Fluid Power, Terrassa, Spain, June30-July 2, 2004, pp. 229-238.

[18] A.T. Schenk, Predicting lubrication performance between the slipper and swashplate in axial piston hydraulic machines, Dissertation from Purdue University, USA, 2014.

[19] H.S. Tang, Y. Ren, J.W. Xiang, A novel model for predicting thermoelastohydrodynamic lubrication characteristics of slipper pair in axial piston pump. International Journal of Mechanical Sciences 124 (2017) 109-121.

[20] J.K. Kim, J.Y. Jung, Measurement of fluid film thickness on the valve plate in oil hydraulic axial piston pumps (I)-bearing pad effects, KSME international journal 17(2) (2003) 246-253.

[21] J.M. Bergada, D.L. Davies, S. Kumar, J. Watton, The effect of oil pressure and temperature on barrel film thickness and barrel dynamics of an axial piston pump, Meccanica 47(3) (2012) 639-654.

[22] S. Wegner, F. Löschner, S. Gels, H. Murrenhoff, Validation of the physical effect implementation in a simulation model for the cylinder block/valve plate contact supported by experimental investigations, in: 10th International Fluid Power Conference, Dresden, Germany, March 8-10, 2016, pp. 269-281.

[23] K. Tanaka, T. Nakahara, K. Kyogoku, Experimental verification of oil whirl of piston in axial piston pump and motor, JSME

International Journal Series C 44(1) (2001) 230-236.
[24] N.D. Manring, Friction forces within the cylinder bores of swash-plate type axial-piston pumps and motors, Journal of dynamic systems, measurement, and control 121(3) (1999) 531-537.
[25] S. Scharf, H. Murrenhoff, Measurement of friction forces between piston and bushing of an axial piston displacement unit, International Journal of Fluid Power 6(1) (2005) 7-17.
[26] L. Olems, Investigations of the temperature behaviour of the piston cylinder assembly in axial piston pumps, International Journal of Fluid Power 1(1) (2000) 27-39.
[27] M. Ivantysynova, R. Lasaar, An investigation into micro-and macrogeometric design of piston/cylinder assembly of swash plate machines, International Journal of Fluid Power 5(1) (2004) 23-36.
[28] H.S. Tang, Y.B. Yin, J. Li, Lubrication characteristics analysis of slipper bearing in axial piston pump considering thermal effect, Lubrication Science 28(2) (2016) 107-124.
[29] N.A. Spencer, Design and development of a novel test method to measure the slipper/swashplate interface fluid film in a positive displacement machine, Dissertation from Purdue University, USA, 2014.
[30] N.D. Manring, V.S. Mehta, B.E. Nelson, K.J. Graf, J.L. Kuehn, Scaling the speed limitations for axial-piston swash-plate type hydrostatic machines, Journal of Dynamic Systems, Measurement, and Control 136(3) (2014) 031004.
[31] J.M. Bergada, S. Kumar, D.L. Davies, J. Watton, A complete analysis of axial piston pump leakage and output flow ripples, Applied Mathematical Modelling 36(4) (2012) 1731-1751.
[32] N.D. Manring, Fluid Power Pumps and Motors: Analysis, Design and Control, McGraw Hill Professional, 2013.
[33] J.H. Shin, K.W. Kim, Effect of surface non-flatness on the lubrication characteristics in the valve part of a swash-plate type axial piston pump, Meccanica 49(5) (2014) 1275-1295.